ZEITSCHRIFT
FÜR PHYSIK D

Optically enhanced magnetic resonance for the study of atom-surface interaction

Stefan Grafström*, Dieter Suter**

Institute of Quantum Electronics, ETH Hönggerberg, CH-8093 Zürich, Switzerland

Received: 11 January 1996

Abstract. We study surface-induced spin relaxation with a laser-assisted magnetic resonance experiment. Optical pumping with polarization-modulated light in a transverse magnetic field creates the spin polarization. For detection a probe laser beam is reflected at the surface and the change of its polarization is monitored. We present a comprehensive theoretical description, taking into account the spin relaxation at the surface, which leads to a spatially inhomogeneous magnetization near the surface as a result of the transient behavior of the atoms in this region. Analytical expressions are derived for the magnetic resonance signal, which show that the wall relaxation causes a clear modification of the line shape, characterized by pronounced wings. The experimental results obtained with bare and silicone-coated Pyrex-glass surfaces are well described by the theory. The bare glass surface causes strong relaxation, whereas the silicone-coated surface is only weakly depolarizing. The analysis of the magnetic-resonance line shape indicates that the depolarization probability per wall collision is ~ 0.01 in the latter case. The results are compared with corresponding results from the analysis of the optical resonance line measured with the same setup. Both types of measurements can be interpreted within the same theoretical framework and are fully consistent with one another.

PACS: 34.50.Dy; 32.30.Dx; 32.70.Jz

I. Introduction

Atomic and molecular spins located close to an interface experience additional interactions not present in the volume and can therefore be used as probes for the investigation of surfaces. Such interactions may originate from a redistribution of electrons inside a molecule that is physisorbed or chemically bonded to the interface [1], or they may be caused by electromagnetic fields at the surface which couple to the spins, e.g. through the nuclear quadrupole interaction [2–4]. These interactions affect the evolution of the spins and can be measured through the magnetic resonance spectrum. Besides shifts of the positions of the magnetic resonance lines, they often cause relaxation, which is closely related to the dwell time of the adsorbed atoms and to the hopping rate between different surface sites. Hence, the relaxation provides insight into adsorption-desorption processes and surface diffusion, as was first demonstrated by Bouchiat and Brossel, who studied wall relaxation in optically pumped alkali vapors contained in paraffin-coated glass cells [5, 6].

In the past years, surface interactions of spin-polarized noble-gas nuclei, mainly Xe, have been studied in a number of nuclear-magnetic-resonance (NMR) experiments, which in particular have addressed the quadrupole interaction with electric-field gradients experienced by surface-adsorbed nuclei [2–4]. While conventional NMR on surfaces is restricted to high-surface-area materials such as powders and zeolites [1, 7, 8], these experiments utilize optical methods for creating and detecting the spin polarization, which results in a tremendous enhancement of the sensitivity and makes possible the observation of spins in a dilute atomic vapor. The Xe nuclei are spin-polarized by spin-exchange collisions with optically pumped Rb vapor. The spin precession is then monitored via the Rb magnetization, which is probed optically. Collisions of the atoms with the walls of the container affect the spin evolution and cause a slight change of the magnetic resonance lines. Very high spectral resolution, in addition to the high sensitivity, is a prerequisite for these experiments.

Recently, first NMR experiments on well-defined single-crystal surfaces were reported, in which β-active ^{8}Li nuclei produced with an ion accelerator were adsorbed on the surface [9, 10]. The spin polarization was again created by optical pumping, but detected via the asymmetric

* *Present address*: Physikalisches Institut, Universität Heidelberg, Philosophenweg 12, D-69120 Heidelberg, Germany
** *Present address*: Fachbereich Physik, Universität Dortmund, D-44221 Dortmund, Germany

angular distribution of the emitted electrons. Thus, the sensitivity could be pushed to the extreme submonolayer range.

On the other hand, atom-surface interaction has been investigated also by purely optical spectroscopy in several experiments which take advantage of the fact that the reflectivity of the solid-gas interface is modified by the interaction [11–14]. In such experiments the deexcitation of optically excited atoms by wall collisions and the modification of the optical transitions by long-range van der Waals interaction could be detected.

We have demonstrated that this method of optical reflection spectroscopy can also be applied for studying spin-polarized atoms in the proximity of a solid surface [15–18]. The electronic spin polarization of optically pumped alkali atoms in a buffer gas is detected through the change of polarization that a laser beam undergoes when reflected at the interface. In contrast to earlier experiments on spin-polarized gas phase atoms, only the atoms close to the surface contribute to the signal. In [18] we discussed the optical resonance line observed in this experiment and showed that wall relaxation modifies the line shape in a characteristic way, which allowed us to deduce the depolarization probability per wall collision quantitatively for a bare Pyrex-glass surface. The experiment also allows us to study the magnetic resonance, which is realized by optical pumping with polarization-modulated light in a transverse magnetic field. The present paper is devoted to the detailed analysis of this situation and addresses the question of how wall relaxation influences the shape of the magnetic resonance line.

The paper is organized as follows: After a brief description of the experimental setup in Sect. II we work out the theory and derive a general expression for the magnetic resonance signal in Sect. III. In Sect. IV we discuss the theoretical results as they apply under typical experimental conditions, before we finally present the experimental results in Sect. V. Section VI provides a conclusion and contrasts the results concerning the magnetic and the optical resonance line.

II. Experimental setup

The experiment, whose setup is depicted in Fig. 1, investigates Na vapor close to a glass surface. The vapor is contained in a heated glass cell together with Ar buffer gas, and the interface under study is formed by the vapor on one side and the surface of a glass prism molten directly to the cell on the other side. We use a frame of reference, in which the interface defines the xy-plane. An intense laser beam tuned to the Na D_1 line ($\lambda = 590$ nm), whose polarization is modulated between left and right circular by an electro-optic modulator (EOM), passes through the interface at normal incidence along the z axis and optically pumps the atomic vapor, thus creating a ground-state spin polarization. A static magnetic field is applied along the y axis perpendicularly to the pump beam and forces the atomic spins into precession around the y axis. The polarization modulation together with the transverse magnetic field results in the creation of a macroscopic magnetization that undergoes a forced precession around the y axis at the modulation frequency. Its magnitude shows a resonant enhancement when the modulation frequency is tuned to the Larmor frequency as given by the static magnetic field [19, 20].

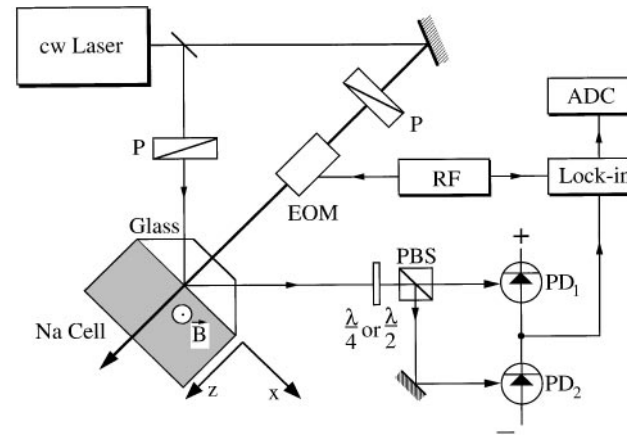

Fig. 1. Experimental setup and definition of the reference frame. *P's*, polarizers; *EOM*, electro-optic modulator; *RF*, frequency synthesizer; *ADC*, analog-to-digital converter; *λ/4 or λ/2*, retardation plate; *PBS*, polarizing beam splitter; *PD's*, photodiodes

The magnetization makes the atomic vapor circularly birefringent. We take advantage of this optical anisotropy for the detection of the precessing magnetization close to the glass surface by reflecting a weak, linearly polarized laser beam off the interface and analyzing its polarization. The precessing magnetization gives rise to a corresponding modulation of the polarization of the reflected probe beam, which is detected with a differential photodetector that measures the intensity difference between two orthogonally polarized components of the light [21, 22]. The signal is demodulated with a lock-in amplifier. The reflected beam probes only a thin layer of the atomic vapor close to the interface, whose thickness is of the order of the optical wavelength, and thus ensures a high surface selectivity [16]. The angle of incidence is chosen close to the critical angle of total internal reflection, θ_c, and can be varied around θ_c within roughly $\pm$ 10 mrad with a resolution of ~ 0.1 mrad with the aid of mirrors mounted on rotational and translational stages driven by stepper motors.

Spin relaxation at the surface decreases the steady-state magnetization close to the wall and leads to the formation of an optically inhomogeneous layer. This spatial inhomogeneity of the medium is probed by the reflected beam and influences the measured signal in a characteristic way. On one hand, information about the surface-induced spin relaxation can be extracted from the strength and shape of the optical resonance, as recorded when the laser frequency is scanned across the D_1 line with the modulation frequency set to the Larmor frequency. We discussed this aspect of the experiment in detail in [18]. In the present paper, we discuss a different experiment: here, we keep the laser frequency constant and acquire the magnetic resonance spectrum by tuning the modulation frequency across the Larmor frequency. In particular, we discuss the modification of the magnetic

resonance line by relaxation processes at the surface. The analysis of this experimental situation requires a more general treatment of the behavior of the magnetization under the combined action of optical pumping, magnetic field, diffusion in the buffer gas, and spin relaxation at the surface.

The experiments on the magnetic resonance were performed with the same two cells that were also used for the study of the optical line in [18], so the results may be compared directly. In one cell the Pyrex-glass surface was directly exposed to the atomic vapor, whereas the other one was coated by a layer of polydimethylsiloxane [23, 24]. The bare glass surface causes strong spin relaxation, whereas the silicone-coated surface affects the spin polarization only weakly, so the two surfaces are well suited as model systems, representing two rather extreme cases. The preparation of the cells has been described elsewhere [16].

The cell temperature was ~ 510–550 K corresponding to a Na number density of roughly 10^{16}–10^{17} m^{-3} as estimated from the optical absorption of the sample. At the operating temperature the buffer gas pressure was ~ 220–240 mbar. The pump beam had an intensity of ~ 5–100 mW/cm^2, whereas the probe beam intensity was ~ 2–4 mW/cm^2. The strength of the magnetic field was set to $\sim 42\,\mu$T corresponding to a Larmor frequency of ~ 300 kHz. The Earth's magnetic field was compensated for by three orthogonal pairs of Helmholtz coils.

III. Theory

A. Outline

We neglect the hyperfine structure and describe the D_1 transition of the Na atoms in the $J = 1/2 \leftrightarrow J' = 1/2$ model, which involves two electronic states with angular momentum $J = 1/2$, each containing two Zeeman sublevels. The neglection of the hyperfine structure as well as the Doppler effect is justified by the presence of the buffer gas that causes a strong pressure broadening, resulting in a homogeneous line width of ~ 4 GHz, which exceeds the hyperfine structure splittings and the Doppler width. To calculate the reflection signal we must first derive the precessing ground-state magnetization, which forms in the steady state as a consequence of the interplay of optical pumping, magnetic field, relaxation in the buffer gas and at the surface, and diffusion of the atoms in the buffer gas. The magnetization follows from the ground-state density matrix, which is found as the stationary solution of the equation of motion in the rotating-wave approximation. The wall relaxation enters the problem via the boundary condition, as it determines the imbalance between incoming and outgoing polarized atoms at the surface. It gives rise to a spatial inhomogeneity, so the magnetization varies as a function of the distance z from the wall. From this z dependence we calculate the reflectivity of the interface and finally arrive at an expression for the signal measured by the polarization-sensitive detector.

B. Equation of motion

In the presence of the buffer gas the populations and coherences of the excited state can be neglected due to their fast decay, so the system can be reduced to the two Zeeman sublevels of the ground state. In this limit the optical pumping may be described by simple rate terms. Let P_+ denote the optical pump rate associated with the left circular component (σ_+) of the pump beam and P_- the corresponding pump rate originating from the σ_- component. For the description of the ground-state dynamics the following contributions must be taken into account [19, 20]:

(*i*) An effective Hamiltonian that describes the influence of the external magnetic field in y direction and the light shift caused by the pump beam, which corresponds to an effective magnetic field along the direction of the pump beam (z direction).

$$H = -\hbar\Omega_L S_y + \hbar\frac{\Delta}{\Gamma}(P_+ - P_-)S_z. \tag{1}$$

Here, S_y and S_z are Pauli spin operators. The Larmor frequency in the external magnetic field is denoted by Ω_L, Δ refers to the detuning of the laser frequency ω_{las} from the optical transition frequency ω_0 ($\Delta = \omega_0 - \omega_{\text{las}}$), and Γ is the optical dephasing rate. The first term in (1) describes the external magnetic field, and the second term originates from to the light shift.

(*ii*) An effective damping of the population difference and the ground-state coherences, driving the system toward thermal equilibrium, which is described by the rate constant

$$\gamma_{\text{eff}} = \gamma + P_+ + P_-. \tag{2}$$

This damping is the combined effect of the pump light ($P_+ + P_-$) and other effects, such as depolarizing collisions with buffer gas atoms and radiation trapping, etc., which are subsumed under γ.

(*iii*) The polarizing effect of the pump beam, which is given by the difference of the two pump rates and builds up a population difference between the Zeeman sublevels.

(*iv*) A diffusion term which describes the change of the density matrix at a given distance z from the interface caused by diffusion of atoms into and out of this layer.

Taking all these contributions into account, we can write the equation of motion, which describes the time evolution of the ground-state density matrix ρ, in the following form:

$$\frac{\partial\rho}{\partial t} = \underbrace{-\frac{i}{\hbar}[H,\rho]}_{(i)} \underbrace{-\gamma_{\text{eff}}\left(\rho - \frac{1}{2}1\right)}_{(ii)} + \underbrace{(P_+ - P_-)S_z}_{(iii)} + \underbrace{D\frac{\partial^2\rho}{\partial z^2}}_{(iv)}. \tag{3}$$

where D denotes the coefficient of diffusion. We assume that the polarization of the pump beam is modulated sinusoidally between left and right circular polarization, so the pump rates can be expressed as:

$$P_{\pm} = \frac{P_0}{2}(1 \pm \cos(\omega_{\mathrm{rf}} t)). \tag{4}$$

Then, the effective damping constant becomes $\gamma_{\mathrm{eff}} = \gamma + P_0$, and the net pump rate is $P_+ - P_- = P_0 \cos(\omega_{\mathrm{rf}} t)$. We transform the equation of motion into a frame of reference that rotates at the modulation frequency around the direction of the external magnetic field. This is accomplished by the unitary transformation

$$U = \exp(-i\omega_{\mathrm{rf}} t S_y), \tag{5}$$

which transforms the Hamiltonian according to

$$H \to H^r = UHU^{-1} + i\hbar \dot{U} U^{-1} = -\hbar\delta S_y + \hbar\delta_0 S_z \tag{6}$$

where we have omitted terms oscillating at $2\omega_{\mathrm{rf}}$ (rotating-wave approximation) and introduced the abbreviations

$$\delta = \Omega_L - \omega_{\mathrm{rf}}$$

$$\delta_0 = \frac{P_0}{2}\frac{\Delta}{\Gamma}. \tag{7}$$

They refer to the detuning of the modulation frequency from the Larmor frequency and to the light shift, respectively. In the rotating frame of reference the equation of motion within the rotating-wave approximation finally becomes:

$$\frac{\partial \rho^r}{\partial t} = -\frac{i}{\hbar}[H^r, \rho^r] - \gamma_{\mathrm{eff}}\left(\rho^r - \frac{1}{2}1\right) + \frac{P_0}{2} S_z + D\frac{\partial^2 \rho^r}{\partial z^2}. \tag{8}$$

We expand the density matrix in terms of spin matrices:

$$\rho^r = \frac{1}{2}1 + m_x^r S_x + m_y^r S_y + m_z^r S_z. \tag{9}$$

The expansion coefficients are the components of the magnetization in the rotating frame ($m_i^r = \mathrm{Tr}(\rho^r S_i)$, $i = x, y, z$). We are seeking the stationary solution of the equation of motion, for which ρ^r becomes time-independent. The condition $\dot{\rho}^r = 0$ leaves us with a set of ordinary differential equations:

$$-D\frac{\mathrm{d}^2}{\mathrm{d}z^2}\begin{pmatrix} m_x^r \\ m_y^r \\ m_z^r \end{pmatrix} = \begin{pmatrix} -\gamma_{\mathrm{eff}} & -\delta_0 & -\delta \\ \delta_0 & -\gamma_{\mathrm{eff}} & 0 \\ \delta & 0 & -\gamma_{\mathrm{eff}} \end{pmatrix}\begin{pmatrix} m_x^r \\ m_y^r \\ m_z^r \end{pmatrix} + \begin{pmatrix} 0 \\ 0 \\ P_0/2 \end{pmatrix}. \tag{10}$$

The ansatz $\mathbf{m}^r = \boldsymbol{\mu}\exp(-\lambda z)$ for the solution of the corresponding homogeneous set of equations delivers the following values of λ:

$$\lambda_1 = \sqrt{\gamma_{\mathrm{eff}}/D} = \mu \tag{11a}$$

$$\lambda_{2/3} = \sigma \exp(\mp i\vartheta) \tag{11b}$$

with the abbreviations:

$$\Omega = \sqrt{\delta^2 + \delta_0^2} \tag{12a}$$

$$\vartheta = (1/2)\arctan(\Omega/\gamma_{\mathrm{eff}}) \tag{12b}$$

$$\sigma = \sqrt{\frac{\sqrt{\gamma_{\mathrm{eff}}^2 + \Omega^2}}{D}}. \tag{12c}$$

Values of λ with a negative real part have been omitted as they represent unphysical solutions, for which the magnetization increases exponentially toward infinity with increasing distance from the interface. Note that we name λ_1 also μ to stay consistent with the notation used in [18]. The eigenvectors belonging to $\lambda_{1/2/3}$ can be expressed as

$$\boldsymbol{\mu}_1 = \begin{pmatrix} 0 \\ \delta \\ -\delta_0 \end{pmatrix} \quad \text{and} \quad \boldsymbol{\mu}_{2/3} = \begin{pmatrix} \pm i\Omega \\ \delta_0 \\ \delta \end{pmatrix}. \tag{13}$$

From the condition $\mathrm{d}^2/\mathrm{d}z^2 = 0$ we obtain the asymptotic solution of (10) for $z \to \infty$:

$$\mathbf{m}_\infty^r = \frac{P_0}{2\gamma_{\mathrm{eff}}(\gamma_{\mathrm{eff}}^2 + \Omega^2)}\begin{pmatrix} -\gamma_{\mathrm{eff}}\delta \\ -\delta_0\delta \\ \gamma_{\mathrm{eff}}^2 + \delta_0^2 \end{pmatrix}. \tag{14}$$

The general solution of (10) can now be written as

$$\mathbf{m}^r(z) = \mathbf{m}_\infty^r + \sum_{i=1}^{3} c_i \boldsymbol{\mu}_i \exp(-\lambda_i z). \tag{15}$$

The coefficients c_i have to be determined from the boundary condition.

C. Boundary condition

To find the proper boundary condition we must consider the origin of the magnetization at the interface ($z = 0$). The atoms at this location are either atoms arriving at the wall by diffusion from deeper layers or atoms leaving the wall after a wall collision or an adsorption-desorption process. The magnetization $\mathbf{m}_{\mathrm{in}}^r$ carried to the interface by the atoms arriving from the bulk is obtained from the following arguments: Be $p(z)\,\mathrm{d}z$ the probability that an atom arriving at the wall has travelled a distance z in z direction since its last collision with a buffer gas atom. Then, assuming that – on average – an atom that has suffered its last collision at a distance z from the interface contributes to the magnetization according to the value of $\mathbf{m}^r(z)$ at that distinct z coordinate, we obtain the relationship:

$$\mathbf{m}_{\mathrm{in}}^r = \int_0^\infty \mathbf{m}^r(z) p(z)\,\mathrm{d}z. \tag{16}$$

Under typical experimental conditions the decay lengths $1/\lambda_i$ with λ_i given by (11) are large compared with the mean free path L_{free} of the Na atoms in the buffer gas (in our case $L_{\mathrm{free}} \approx 0.9$ μm and $\lambda_1^{-1} \approx 56$ μm, see section IV). This is indeed an essential prerequisit for the validity of the diffusion term in (8). Therefore, the magnetization can

be well approximated by a linear function of z on the length scale of the mean free path. As $p(z)$ falls off within a few L_{free}, we can therefore consider $\mathbf{m}^r$ as a linear function of z in the integral of (16). Hence, the average defined by (16) may be replaced by the magnetization at an average distance L:

$$\mathbf{m}^r_{\text{in}} = \mathbf{m}^r(L) \text{ with } L = \int_0^\infty zp(z)\,\mathrm{d}z = 2/3\,L_{\text{free}}. \tag{17}$$

The numerical value $2/3\ L_{\text{free}}$ is valid under the assumption that the distribution of free paths is exponential, and isotropic in space [25]. Note that L is simply the average distance that an atom arriving at the interface has travelled in z direction since its last collision.

The atoms that leave the surface originally carried the same average magnetization as above when they arrived at the surface. However, because of disorientation by the interaction with the surface, their magnetization has been reduced by a factor $1-\varepsilon$, where ε denotes the probability that an atom is depolarized upon collision with the surface:

$$\mathbf{m}^r_{\text{out}} = (1-\varepsilon)\mathbf{m}^r_{\text{in}} = (1-\varepsilon)\mathbf{m}^r(L). \tag{18}$$

Finally, the total magnetization at the interface ($z=0$) is given by the sum of the contributions of arriving and leaving atoms, which both represent one half of the total number of atoms:

$$\mathbf{m}^r(0) = \frac{2-\varepsilon}{2}\,\mathbf{m}^r(L). \tag{19}$$

The depolarizing atom-surface interaction enters the theory via this relationship, which provides the boundary condition necessary to determine the coefficients c_i of (15). With the approximation $\mathbf{m}^r(L) = \mathbf{m}^r(0) + L(\mathrm{d}\mathbf{m}^r/\mathrm{d}z)(0)$ the boundary condition can also be expressed as

$$\frac{\mathrm{d}\mathbf{m}^r}{\mathrm{d}z}(0) = \frac{\varepsilon}{(2-\varepsilon)L}\,\mathbf{m}^r(0) \tag{20}$$

which is in complete agreement with the expression given by Masnou-Seeuws and Bouchiat [26]. Here we have assumed that the surface interaction diminishes the magnitude of the magnetization without changing its direction in the rotating frame, i.e., without changing the phase of the precessing magnetization. In a more general situation of coherent wall interaction the influence of the wall cannot be described by a scalar and (18) has to be replaced by a modified expression [27].

D. Stationary magnetization

The solution of (10) that satisfies the boundary condition given by (20) reads as:

$$\mathbf{m}^r(z) = \mathbf{m}^r_\infty + \frac{P_0\delta_0}{2\gamma_{\text{eff}}\Omega^2} \times \frac{\exp(-\mu z)}{1+\dfrac{2-\varepsilon}{\varepsilon}\,\mu L} \begin{pmatrix} 0 \\ \delta \\ -\delta_0 \end{pmatrix}$$

$$+ \frac{P_0\gamma_{\text{eff}}\delta}{2\Omega^2(\gamma_{\text{eff}}^2+\Omega^2)}\,A\exp(-\sigma z\cos\vartheta)$$

$$\times \left\{ \cos(\sigma z\sin\vartheta) \begin{pmatrix} q\Omega \\ -p\delta_0 \\ -p\delta \end{pmatrix} + \sin(\sigma z\sin\vartheta) \begin{pmatrix} p\Omega \\ q\delta_0 \\ q\delta \end{pmatrix} \right\} \tag{21}$$

with

$$A = \left(1 + 2\,\frac{2-\varepsilon}{\varepsilon}\,\sigma L\cos\vartheta + \left(\frac{2-\varepsilon}{\varepsilon}\,\sigma L\right)^2\right)^{-1} \tag{22a}$$

$$p = 1 + \frac{2-\varepsilon}{\varepsilon}\,\sigma L\cos\vartheta - \frac{\Omega}{\gamma_{\text{eff}}} \times \frac{2-\varepsilon}{\varepsilon}\,\sigma L\sin\vartheta \tag{22b}$$

$$q = \frac{\Omega}{\gamma_{\text{eff}}}\left(1 + \frac{2-\varepsilon}{\varepsilon}\,\sigma L\cos\vartheta\right) + \frac{2-\varepsilon}{\varepsilon}\,\sigma L\sin\vartheta. \tag{22c}$$

To complete the calculation of the stationary magnetization, we transform the result from the rotating frame of reference back to the laboratory frame and obtain:

$$\mathbf{m} = \begin{pmatrix} m^r_x\cos(\omega_{\text{rf}}t) - m^r_z\sin(\omega_{\text{rf}}t) \\ m^r_y \\ m^r_z\cos(\omega_{\text{rf}}t) + m^r_x\sin(\omega_{\text{rf}}t) \end{pmatrix}. \tag{23}$$

Thus, we have finally arrived at an explicit expression for the magnetization $\mathbf{m}$, which rotates around the y axis at the modulation frequency ω_{rf}. As a consequence of the relaxation at the surface, the amplitude and phase of the precessing magnetization vary with the distance from the surface, so the medium is spatially inhomogeneous. It is rather instructive to visualize the z dependence for different cases. The situation becomes especially simple if the radio frequency is exactly on resonance ($\delta = 0$). Then m^r_x and m^r_y vanish for all values of z, which means that in the laboratory frame $\mathbf{m}$ rotates in the xz plane with only the amplitude but not the phase depending on z. In this case the oscillation of m_z is always in phase with the polarization modulation of the pump beam ($\propto \cos(\omega_{\text{rf}}t)$), with m_z reaching its extreme values each time the polarization passes through a state of purely circular polarization. The z dependence is given by a simple exponential approach of the magnetization toward its bulk value as illustrated in Fig. 2a [17, 18].

In the general case of off-resonance excitation both the amplitude and the phase vary with z. Figure 2b shows the behavior of m^r_x and m^r_z for an rf detuning $\delta = -5\gamma_{\text{eff}}$ under the assumption that each wall collision is completely disorienting ($\varepsilon = 1$). The most striking feature is that the magnetization does not just rise continuously toward the bulk value but goes through a maximum. At this distance from the surface, the magnetization is higher than in the bulk, despite the depolarization at the surface. The reason for this phenomenon can be traced back to a corresponding behavior in the time domain. When an atom is completely depolarized at the surface and returns back to the gas phase, it shows a transient behavior during the period when the polarization is built up again by optical pumping before reaching the steady state. If the radio frequency is off resonance, this transient regime is typically characterized by a damped oscillation of the amplitude and phase, as illustrated by Fig. 3, which shows the temporal evolution of the magnetization in the

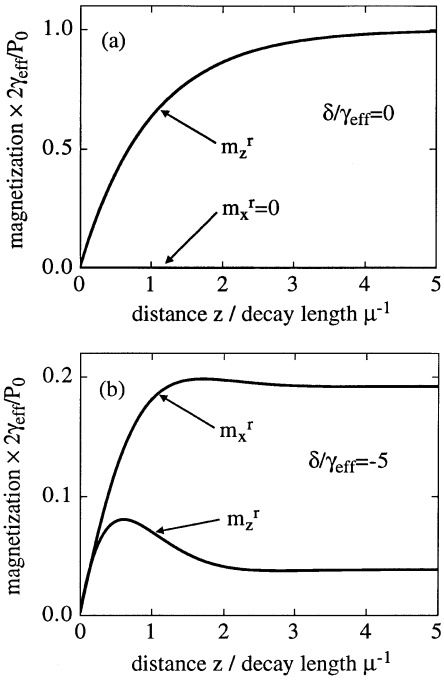

Fig. 2a, b. Magnetization in the rotating reference frame as a function of the distance z from the wall for on-resonance (**a**) and off-resonance (**b**) radio frequency excitation. The x and z components of the magnetization vector are plotted separately. They have been normalized to the on-resonance bulk value $P_0/(2\gamma_{\mathrm{eff}})$. The distance z is given in units of the decay length μ^{-1}, which describes the exponential curve shown in (**a**)

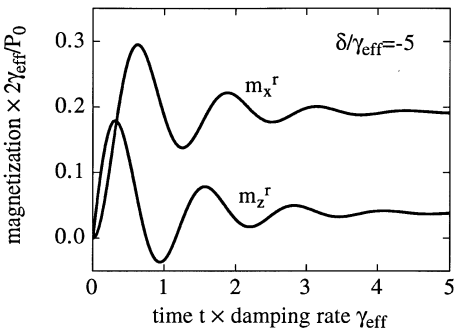

Fig. 3. Transient behavior of the magnetization (represented by its normalized x and z components in the rotating frame) in the time domain under the action of polarization-modulated optical pumping under off-resonance conditions. The time is given in units of the inverse effective damping rate

rotating frame, starting from complete depolarization. The variation of the steady state magnetization in space (Fig. 2b) is a remnant of this temporal behavior. Near the surface a large fraction of the atoms is in the transient time regime, since only a comparably short period of time has elapsed since they suffered their last wall collision. As the magnetization at a certain distance from the surface is the sum of the contributions of a large number of atoms with different individual histories as a result of the diffusive motion, the temporal oscillations seen in Fig. 3 are washed out in space, so only the much weaker spatial oscillations of Fig. 2b remain.

E. Signal

The signal measured by the polarization-sensitive detector can be calculated from the reflection matrix, which relates the *s*- and *p*-polarized amplitudes of the electric field of the incident wave to their reflected counterparts. In [18], we discussed this calculation in detail and showed that the signal is determined by the off-diagonal elements of the reflection matrix, which describe the transformation of one component of polarization (*s* or *p*) to the orthogonal one upon reflection at the interface. In the case of a one-dimensionally inhomogeneous medium the matrix elements can be calculated analytically to first order in terms of the tensor of optical susceptibility [28, 18]. For spin-polarized sodium vapor the following expressions are obtained for the relevant matrix elements [18]:

$$\delta r_{\mathrm{ps/sp}} = w\chi_0 \left\{ \xi m_z(0) \mp \eta m_x(0) + \int_0^\infty \mathrm{e}^{\mathrm{i}2k_0\xi z} \frac{\mathrm{d}}{\mathrm{d}z}\left[\xi m_z(z) \mp \eta m_x(z)\right] \mathrm{d}z \right\} \quad (24)$$

with

$$\eta = n_0 \sin\theta_i \quad (25a)$$

$$\xi = \sqrt{1 - (n_0 \sin\theta_i)^2} \quad (25b)$$

$$w = \frac{i n_0 \cos\theta_i}{\xi(\cos\theta_i + n_0\xi)(n_0\cos\theta_i + \xi)} \quad (25c)$$

where n_0 is the index of refraction of the glass prism, θ_i the angle of incidence at the interface, k_0 the vacuum wave vector, and χ_0 the susceptibility of the unpolarized sodium vapor, which we assume to have a Lorentzian dependence on the laser detuning. The upper sign in (24) applies to δr_{ps} and the lower one to δr_{sp}. Note that η and ξ are the sine and the cosine of the angle of refraction θ_t according to Snell's law for the case that the atomic vapor is replaced by vacuum. In the case of total internal reflection ξ becomes purely imaginary, whereas η is always real. With the magnetization according to (23) we can now rewrite the elements of the reflection matrix in the following way:

$$\delta r_{\mathrm{ps/sp}} = w\chi_0 \{\cos(\omega_{\mathrm{rf}} t)(\xi M_z \mp \eta M_x) + \sin(\omega_{\mathrm{rf}} t)(\xi M_x \pm \eta M_z)\} \quad (26)$$

where M_x and M_z are defined by

$$M_j = m^r_{\infty j} + i2k_0\xi \int_0^\infty \mathrm{e}^{\mathrm{i}2k_0\xi z}(m^r_{\infty j} - m^r_j(z))\,\mathrm{d}z \quad (27)$$

with $i = x, z$. The integral of (27) was rewritten after integration by parts to obtain a form which is more suited to be evaluated with the expression of (21). The evaluation

yields:

$$M_x = -\frac{P_0}{2\gamma_{\text{eff}}} \times \frac{\delta\gamma_{\text{eff}}}{\gamma_{\text{eff}}^2 + \Omega^2} \left\{ 1 + \frac{\gamma_{\text{eff}}}{\Omega} A(qC + pS) \right\} \tag{28a}$$

$$M_z = \frac{P_0}{2\gamma_{\text{eff}}} \left\{ \frac{\gamma_{\text{eff}}^2 + \delta_0^2}{\gamma_{\text{eff}}^2 + \Omega^2} + \frac{\gamma_{\text{eff}}^2}{\gamma_{\text{eff}}^2 + \Omega^2} \times \frac{\delta^2}{\Omega^2} A(pC - qS) + \frac{\delta_0^2}{\Omega^2} \times \frac{E}{1 + \dfrac{2-\varepsilon}{\varepsilon} \mu L} \right\} \tag{28b}$$

with

$$C = -\frac{1 + i \dfrac{\sigma}{2k_0\xi} \cos\vartheta}{1 + i \dfrac{\sigma}{k_0\xi} \cos\vartheta - \left(\dfrac{\sigma}{2k_0\xi} \right)^2} \tag{29a}$$

$$S = -\frac{i \dfrac{\sigma}{2k_0\xi} \sin\vartheta}{1 + i \dfrac{\sigma}{k_0\xi} \cos\vartheta - \left(\dfrac{\sigma}{2k_0\xi} \right)^2} \tag{29b}$$

$$E = -\frac{1}{1 + i \dfrac{\mu}{2k_0\xi}} . \tag{29c}$$

Below, we concentrate on the case that the probe beam is *s*-polarized and the detector measures the intensity difference between the linearly polarized components of the reflected beam oriented at $\pm 45^\circ$ with respect to the plane of incidence. As shown in [18], for this configuration the signal (i.e., the modulated part of the measured intensity difference normalized to the total intensity of the probe beam) is given by

$$s = \text{Re}\{2r_{s0}^* \delta r_{\text{ps}}\}, \tag{30}$$

where r_{s0} denotes the Fresnel coefficient of reflection for *s*-polarized light at an interface between glass and vacuum for the given angle of incidence [29], and the asterisk refers to complex conjugation. Other configurations of probe beam polarization and detector arrangement can also be used, but provide no additional information [18]. On the basis of (26) we can now split the signal into an in-phase part s_{ip} (whose time dependence is given by $\cos(\omega_{\text{rf}} t)$) and an out-of-phase part s_{op} ($\propto \sin(\omega_{\text{rf}} t)$).

$$s_{\text{ip}} = \text{Re}\{2r_{s0}^* w\chi_0(\xi M_z - \eta M_x)\} \tag{31a}$$

$$s_{\text{op}} = \text{Re}\{2r_{s0}^* w\chi_0(\eta M_z + \xi M_x)\}. \tag{31b}$$

These expressions provide a full description of the signal and allow us to analyze its dependence on various parameters, such as detunings of the probe and pump laser frequencies or the modulation frequency, angle of incidence, and depolarization probability. In the following, we shall consider a number of important limiting cases, in which the theoretical expressions reduce to considerably simpler formulas, which facilitate a clearer understanding of various dependences. In particular, we shall work out which quantities give experimental access to the depolarization probability.

IV. Discussion of the theory

A. Experimental conditions

First of all, it is helpful to get an overview over some typical numbers as they apply to our experiment. This will allow us to further simplify the theoretical results of the preceding section. We used a buffer gas pressure of ~ 230 mbar of Argon at a temperature of ~ 540 K, which gives a diffusion coefficient of $\sim 2\,\text{cm}^2/\text{s}$ [30], corresponding to a mean free path $L_{\text{free}} = 0.9\,\mu\text{m}$. The magnetic field was chosen to provide a Larmor frequency of ~ 300 kHz, and the modulation frequency was varied between 200 and 400 kHz, corresponding to a maximum rf detuning $\delta_{\max}$ of $\pm 2\pi \times 100$ kHz. As this is much more than the maximum pump rate used in the experiment (which is confirmed by the analysis of the rf lineshape, see Sect. V) the maximum value of σ is $\approx (\delta_{\max}/D)^{1/2} \approx 6 \times 10^4\,\text{m}^{-1}$. Close to the critical angle of total internal reflection θ_c, the parameter ξ is related to the detuning $\theta_i - \theta_c$ between the angle of incidence and the critical angle by

$$\xi^2 = -2(\theta_i - \theta_c)\sqrt{n_0^2 - 1}. \tag{32}$$

Hence, the condition

$$\left| \frac{\sigma}{k_0\xi} \right| \ll 1 \tag{33a}$$

is equivalent to

$$|\theta_i - \theta_c| \gg \frac{1}{2\sqrt{n_0^2 - 1}} \left(\frac{\sigma}{k_0} \right)^2 = 1.4 \times 10^{-5}\,\text{rad} \tag{33b}$$

where the above value of σ, a wavelength of 590 nm (D_1 line of Na), and a refractive index $n_0 = 1.5$ were assumed. For a straightforward interpretation of the data we must restrict the measurements to angular detunings well above the divergence of the probe laser beam, which is much larger than 14 μrad. Therefore, we can obviously consider $\sigma/(k_0\xi)$ as a small quantity for all practical purposes. As μ is always smaller than σ, this also applies to $\mu/(k_0\xi)$. Therefore, we may expand C, S, and E to first order in terms of these small quantities and obtain:

$$C = -1 + i \frac{\sigma}{2k_0\xi} \cos\vartheta \tag{34a}$$

$$S = -\frac{i\,\sigma}{2k_0\xi} \sin\vartheta \tag{34b}$$

$$E = -1 + i \frac{\mu}{2k_0\xi} . \tag{34c}$$

We will use these approximations throughout the paper in the following.

B. Modulation frequency on resonance ($\delta = 0$)

In [18] we discussed the properties of the optical resonance line, as recorded when the laser frequency is tuned while the modulation frequency is kept on resonance. Therefore, the first question we address here concerns the consistency of the expressions derived above with our earlier results. If the modulation frequency coincides with the Larmor frequency ($\delta = 0$), (28) together with (34) yields:

$$M_x = 0 \tag{35a}$$

$$M_z = \frac{P_0}{2\gamma_{\text{eff}}}\, g_0 \left(1 + \frac{\varepsilon}{2-\varepsilon} \times \frac{i}{2k_0 L \xi}\right) \tag{35b}$$

with

$$g_0 = \frac{\dfrac{2-\varepsilon}{\varepsilon}\,\mu L}{1 + \dfrac{2-\varepsilon}{\varepsilon}\,\mu L}. \tag{36}$$

The prefactor $P_0/(2\gamma_{\text{eff}})$ in (35) represents the amplitude $m_\infty = |\mathbf{m}^r_\infty|$ of the rotating magnetization in the bulk, i.e. for $z \to \infty$ (see (14)). From (21) we see that $m_\infty g_0$ is the corresponding amplitude at the surface ($z = 0$). With the definition $v = 2r^*_{s0} w \eta M_z / m_\infty$, the out-of-phase signal can now be written as $s_{\text{op}} = \text{Re}\{m_\infty \chi_0 v\}$ in agreement with the expression derived in [18]. The only difference is that the complete treatment presented in this paper yields $m_\infty = P_0/(2\gamma_{\text{eff}})$ (with a saturation value of 1/2 for $P_0 \to \infty$), whereas the simpler treatment of [18], which did not take into account the detailed mechanism of polarization-modulated optical pumping, gave $m_\infty = P_0/\gamma_{\text{eff}}$ (with a saturation value of 1, corresponding to complete polarization). This deviation is, however, irrelevant for the discussion and the evaluation of the data.

A brief summary of the main points worked out in [18] is helpful for a comparison with the results on the magnetic resonance line presented in the following paragraphs: In [18] we showed that the phase and the absolute value of v determine the shape and the strength of the optical line, respectively. The line exhibits a mixed absorptive-dispersive shape with the mixing angle given by the phase of v. The extent of wall relaxation is reflected by a characteristic dependence of the line shape on the angle of incidence immediately below the critical angle of total internal reflection. From this dependence the depolarization probability can be deduced quantitatively. For a bare Pyrex-glass surface we found $\varepsilon \approx 0.5$. This method is, however, useful for the determination of ε only for relatively strong wall relaxation. Under our experimental conditions the line shape becomes rather insensitive to ε below $\varepsilon \approx 0.1$. Below we show that the magnetic resonance provides more information about the wall relaxation in this case.

C. Laser on resonance ($\Delta = 0$), partial transmission

We now turn to the magnetic resonance line, i.e., we assume a constant laser frequency and discuss the dependence of the signal on the modulation frequency. The situation becomes easiest to survey if the laser is exactly on resonance and the angle of incidence is below the critical angle. The experimental data presented in section IV were acquired under these conditions. For zero laser detuning ($\Delta = 0$) χ_0 is purely imaginary, and for $\theta_i < \theta_c$ (partial transmission) ξ is real. In this case w becomes purely imaginary, whereas r_{s0} is real. Consequently, $r^*_{s0} w \chi_0$ is real and we can rewrite (31) as

$$s_{\text{ip}} = 2r_{s0} w \chi_0 (\xi\, \text{Re}\{M_z\} - \eta\, \text{Re}\{M_x\}) \tag{37a}$$

$$s_{\text{op}} = 2r_{s0} w \chi_0 (\eta\, \text{Re}\{M_z\} + \xi\, \text{Re}\{M_x\}). \tag{37b}$$

Taking into account that the light shift δ_0 vanishes on resonance, i.e. for $\Delta = 0$, and using the approximations given by (34), we arrive at the following expressions for $\text{Re}\{M_x\}$ and $\text{Re}\{M_z\}$:

$$\text{Re}\{M_x\} = -\frac{P_0}{2\gamma_{\text{eff}}} \times \frac{\delta\gamma_{\text{eff}}}{\gamma^2_{\text{eff}} + \delta^2} \times \left\{ 1 - \frac{1 + \dfrac{2-\varepsilon}{\varepsilon}\,\sigma L \left(\cos\vartheta + \dfrac{\gamma_{\text{eff}}}{\delta}\sin\vartheta\right)}{1 + 2\dfrac{2-\varepsilon}{\varepsilon}\,\sigma L \cos\vartheta + \left(\dfrac{2-\varepsilon}{\varepsilon}\,\sigma L\right)^2} \right\} \tag{38a}$$

$$\text{Re}\{M_z\} = \frac{P_0}{2\gamma_{\text{eff}}} \times \frac{\gamma^2_{\text{eff}}}{\gamma^2_{\text{eff}} + \delta^2} \times \left\{ 1 - \frac{1 + \dfrac{2-\varepsilon}{\varepsilon}\,\sigma L \left(\cos\vartheta - \dfrac{\delta}{\gamma_{\text{eff}}}\sin\vartheta\right)}{1 + 2\dfrac{2-\varepsilon}{\varepsilon}\,\sigma L \cos\vartheta + \left(\dfrac{2-\varepsilon}{\varepsilon}\,\sigma L\right)^2} \right\} \tag{38b}$$

where ϑ and σ have been redefined as

$$\vartheta = (1/2)\arctan(\delta/\gamma_{\text{eff}})$$

$$\sigma = \sqrt{\frac{\sqrt{\gamma^2_{\text{eff}} + \delta^2}}{D}} = \mu(1 + (\delta/\gamma_{\text{eff}})^2)^{1/4}. \tag{39}$$

For $\varepsilon \to 0$ the formulas reduce to the expressions in front of the braces, which describe the dispersive and absorptive component of a Lorentzian line, respectively. They simply correspond to the x and z component of the magnetization $\mathbf{m}^r_\infty$ in the bulk. The expressions in the braces describe the modification of the line caused by wall relaxation.

The key parameter that determines how strongly wall relaxation affects the line shape is $\mu L(2-\varepsilon)/\varepsilon$. It is helpful to map out the range covered by this parameter under typical experimental conditions. For $\gamma_{\text{eff}} = 2\pi \times 10\,\text{kHz}$ and $D = 2 \times 10^{-4}\,\text{m}^2/\text{s}$ we find $\mu^{-1} = 56\,\mu\text{m}$. From the diffusion coefficient and the temperature we estimate the mean free path to be $\sim 0.9\,\mu\text{m}$, so $L = 0.6\,\mu\text{m}$ [18]. With

these values, complete depolarization at the wall ($\varepsilon = 1$) yields $\mu L(2-\varepsilon)/\varepsilon = 0.01$, whereas with $\varepsilon = 0.1$ we find $\mu L(2-\varepsilon)/\varepsilon = 0.2$. Hence, this parameter is well below 1 for strong wall relaxation, but increases rapidly when ε becomes smaller. Figure 4 displays $\mathrm{Re}\{M_z\}$ as a function of the rf detuning for a series of different values of $\mu L(2-\varepsilon)/\varepsilon$, which we have chosen such that they correspond to values of ε between 0 and 1 with μ and L as stated. The figure illustrates that wall relaxation is reflected in a very characteristic way by the magnetic resonance line. The most conspicuous feature is that the wings of the line become more and more pronounced with increasing ε. This phenomenon is directly related to the z dependence of the magnetization discussed in Sect. III.D. In the case of strong wall relaxation, we saw that the magnetization rises more rapidly with z for large rf detuning (i.e. in the wings of the line) than for $\delta = 0$, as a consequence of the transient behavior of the atoms close to the wall. This leads to a comparatively strong signal for large δ and causes the peculiar shape of the magnetic resonance line. We can express the same finding in a different way, considering the absolute signal amplitude: with increasing ε the center of the line is more strongly suppressed than the wings, which results in an enhancement of the wings with respect to the center.

D. *Strong relaxation*

From Fig. 4 we may tentatively infer that the line approaches an asymptotic shape with increasing ε, so the shape becomes more or less independent of ε for strong depolarization at the surface. This is indeed true, as we will now demonstrate. The relevant parameter is again $\mu L(2-\varepsilon)/\varepsilon$ rather than ε itself, and we must consider the case $\mu L(2-\varepsilon)/\varepsilon \ll 1$. Then also $\sigma L(2-\varepsilon)/\varepsilon \ll 1$ holds true unless the rf detuning is too large, and we can make a first-order expansion in terms of $\sigma L(2-\varepsilon)/\varepsilon$. We drop the restrictions of the preceding paragraph with regard to the angle of incidence and the laser detuning and make a completely general analysis, starting from (28) together with the approximations listed in (34). The first-order expansion then yields:

$$M_j = R_j\left(\frac{2-\varepsilon}{\varepsilon} + \frac{i}{2k_0 L\xi}\right), \quad j = x, z \tag{40}$$

where the real quantities R_x and R_z are given by

$$R_x = -\frac{P_0}{2\gamma_{\mathrm{eff}}} \times \frac{\delta\gamma_{\mathrm{eff}}}{\gamma_{\mathrm{eff}}^2 + \Omega^2}\, \sigma L\left(\cos\vartheta - \frac{\gamma_{\mathrm{eff}}}{\Omega}\sin\vartheta\right) \tag{41a}$$

$$R_z = \frac{P_0}{2\gamma_{\mathrm{eff}}}\left\{\frac{\gamma_{\mathrm{eff}}^2}{\gamma_{\mathrm{eff}}^2 + \Omega^2} \times \frac{\delta^2}{\Omega^2}\, \sigma L\left(\cos\vartheta + \frac{\Omega}{\gamma_{\mathrm{eff}}}\sin\vartheta\right) + \frac{\delta_0^2}{\Omega^2}\,\mu L\right\}. \tag{41b}$$

The dependence of the signal on δ is completely contained in R_x and R_z, which are independent of ε. In the case of partial transmission, where η and ξ are both real, the in-phase signal can now be written as

$$s_{\mathrm{ip}} = (\xi R_z - \eta R_x) \times \mathrm{Re}\left\{2r_{s0}^* w\chi_0\left(\frac{2-\varepsilon}{\varepsilon} + \frac{i}{2k_0 L\xi}\right)\right\}. \tag{42}$$

The line shape is given by the real expression $\xi R_z - \eta R_x$, whereas the second factor $\mathrm{Re}\{\ldots\}$ is a constant for a fixed laser detuning and depolarization probability. Hence, ε influences only the amplitude of the signal but not the line shape. On the other hand, for an angle of incidence above the critical angle, ξ is purely imaginary with $\xi = \mathrm{i}|\xi|$ and we get

$$s_{\mathrm{ip}} = \left(\frac{2-\varepsilon}{\varepsilon} + \frac{1}{2k_0 L|\xi|}\right) \times \mathrm{Re}\{2r_{s0}^* w\chi_0(\mathrm{i}|\xi|R_z - \eta R_x)\}. \tag{43}$$

Again a situation arises, in which the expression containing ε only plays the role of a constant prefactor with no influence on the shape of the magnetic resonance line.

Hence, we have established that it is a general feature that for $\mu L(2-\varepsilon)/\varepsilon \ll 1$ no information about the numerical value of ε can be gained from an analysis of the line shape. Whether the angle of incidence is below or above the critical angle and whether the laser is on or off resonance is irrelevant for this result, which applies both to the in-phase and the out-of-phase part of the signal.

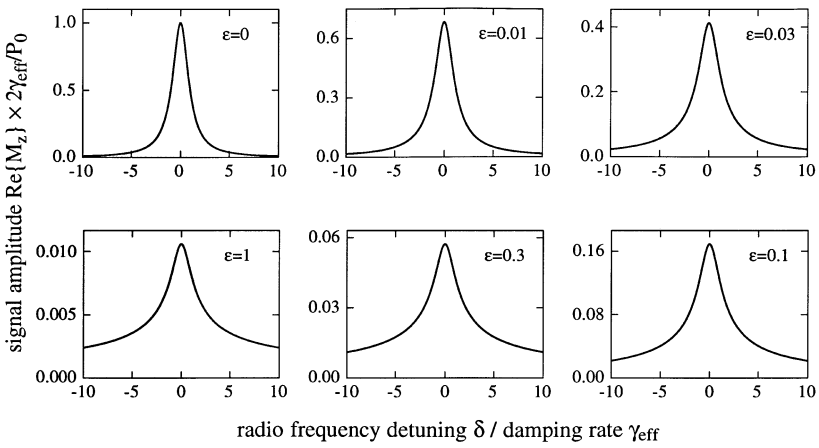

Fig. 4. Signal $\mathrm{Re}\{M_z\}$ as a function of the radio frequency detuning, describing the out-of-phase magnetic resonance signal immediately below the critical angle of total internal reflection for zero laser detuning. Curves for six different values of $\mu L(2-\varepsilon)/\varepsilon$ are shown. Under the assumption $\mu^{-1} = 56\ \mu\mathrm{m}$ and $L = 0.6\ \mu\mathrm{m}$ they correspond to values of the depolarization probability ε per wall collision ranging from 0 to 1. Normalization has been chosen such that $\varepsilon = 0$ gives unity signal amplitude

V. Experimental results

A. General remarks

The signal was extracted with a two-phase lock-in amplifier referenced to the modulation frequency, allowing the simultaneous recording of both the in-phase and the out-of-phase signal. The raw spectra are significantly distorted because of the frequency-dependent phase lag produced by the modulation system and the detector. To correct for these errors we measured the frequency response of the electronics in the following way: The polarization modulation produced by the EOM was transformed to a power modulation by means of a quarter-wave plate and a linear polarizer arranged as a reverse circular polarizer. This power modulation is in phase with the primary polarization modulation, with left and right circular polarization being transformed to zero and maximum power, respectively. The pump beam was then directed onto the differential detector, whose signal was measured with the lock-in amplifier as a function of the modulation frequency. The signal loop thus created contains all elements that are present in the real experiment contributing to the signal distortion. All spectra presented in the following have been corrected correspondingly with respect both to phase shifts and variations of the amplitude.

B. Uncoated cell

We first present the data measured with the uncoated Pyrex-glass cell. Figures 5a and b display the in-phase and the out-of-phase part of the magnetic resonance signal, respectively, as measured slightly below the critical angle of total internal reflection at $\theta_i - \theta_c = -1.2$ mrad. The line is characterized by a rather narrow central feature and very wide wings. The theoretical analysis in the preceding section showed that this appearance is the typical indication of strong wall relaxation. Therefore, we fitted the asymptotic theoretical line shape expected for $\mu L(2-\varepsilon)/\varepsilon \ll 1$ to the data. We fitted both the in-phase and the out-of-phase part simultaneously, minimizing the total χ^2 by describing both curves by a common set of parameters, comprising the effective damping rate γ_{eff}, the pump rate P_0, the center frequency, and the angle of refraction θ_t. A constant background was the only parameter that was adjusted individually for the in-phase and the out-of-phase signal. The data is very well reproduced by the theory (see solid curves in Fig. 5), which confirms that the wall relaxation is so strong that the asymptotic form discussed in Sect. IV.D represents a proper approximation. Using the general expressions of (38) instead and including the depolarization probability ε as a free parameter in the fit turns out to be meaningless, as ε mainly influences the prefactor without affecting the line shape very much. Therefore, it interferes strongly with the pump rate P_0 (which also appears as a prefactor) and consequently the fit produces values of ε and P_0 with extremely large errors, so no useful information about ε can be gained besides the finding that it obviously must be rather large. However, the optical rather than the magnetic line shape provides more accurate information about the strength of the wall relaxation in this case. In [18] we deduced the relaxation probability ε from the charateristic dependence of the optical line shape on the angle of incidence, and we found $\varepsilon \approx 0.5$, in full agreement with the above finding that the magnetic resonance line is well described by the asymptotic theoretical expression of Sect. IV.D.

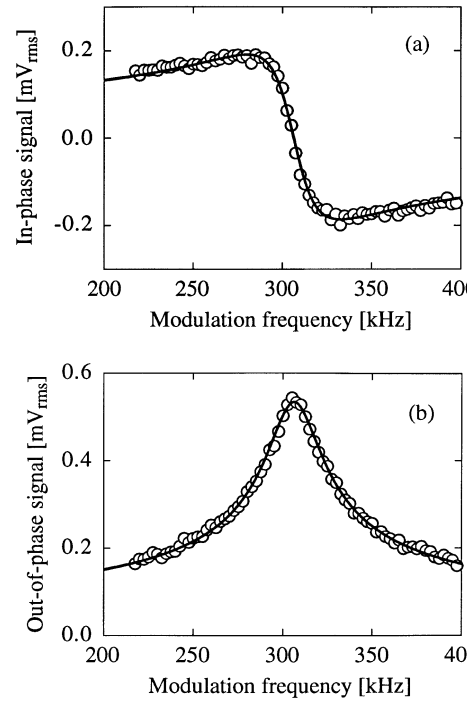

Fig. 5a, b. In-phase (**a**) and out-of-phase (**b**) magnetic resonance signal measured with the uncoated glass cell in the region of partial transmission at a pump power of 10 mW. Only every tenth data point is depicted. The *solid curves* represent a simultaneous least-squares fit of the theory to both signals. Constant backgrounds have been subtracted from the experimental data

The dependence of the magnetic line on the pump power offers an additional possibility for checking the consistency of the theory. Therefore, we recorded the magnetic resonance line for pump powers between 1 mW and 20 mW and extracted the pump rate and the effective damping rate in each case from a fit of the theory to the data in the way described above. The data were taken at an angular detuning $\theta_i - \theta_c = -1.2$ mrad, which corresponds to an angle of refraction $\theta_t = 87°$. The best fit between experiment and theory, however, is obtained for $\theta_t \approx 89.8°$. This deviation can readily be attributed to a misadjustment of the reference phase of the lock-in amplifier by a few degrees. For the evaluation of the power dependence we used a fixed value of $\theta_t = 89.8°$ for all fits, while the other parameters listed above were adjusted each time. Figure 6 displays the results for a data set taken at a temperature of $T = 540$ K. The parameter labelled "pump rate" also incorporates the photodiode sensitivity and the amplifier gain as well as the Na vapor density and the angle of incidence, and is therefore given in arbitrary units. Provided that these quantities stay constant, this parameter should reflect the behavior of the pump rate when the pump power is changed. We expect the pump

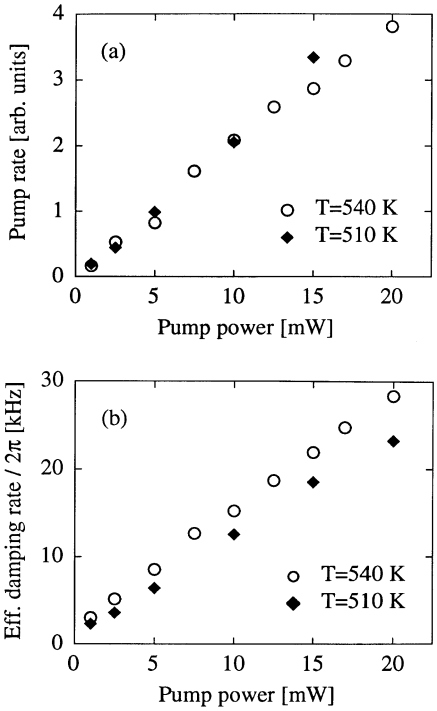

Fig. 6a, b. Pump rate (**a**) and effective damping rate (**b**) as a function of the power of the pump beam. The values were extracted from a fit of the theoretical magnetic line shape to the experiment in each individual case. The *open circles* represent data taken at a temperature of 540 K, whereas the data shown as *black squares* were obtained at 510 K

rate to be directly proportional to the power of the pump laser beam, whereas the effective damping rate $\gamma_{\text{eff}} = \gamma + P_0$ should show a linear dependence on the pump power with an offset given by the intrinsic damping rate γ. Indeed, it is exactly this behavior that we find when describing the experimental data by the theoretical expressions derived above. Thus, the fit of the theory to the experiment not only gives a good agreement in each individual case, but also provides the expected behavior of the parameters as a function of the pump power.

In Fig. 6 we have also inserted data obtained at $T = 510$ K at a Na number density that was a factor of ~ 5 smaller than in the previously described measurement, as estimated from the vapor pressure listed in [31]. The pump rate has been rescaled with respect to the vapor density and the angle of incidence, so the two data sets can be compared directly. We find that the pump rates of both measurements coincide rather well, whereas there is a clear difference with respect to the effective damping rate. While an extrapolation to zero pump power delivers essentially the same value γ_0 in both cases the damping rate increases more slowly with the pump power for $T = 510$ K than for $T = 540$ K. We interpret this as an indication that radiation trapping, i.e., reabsorption of fluorescence light, plays a major role as a damping mechanism [32, 33]. Then, γ can be split into a part γ_0 mainly caused by collisions with buffer gas atoms or impurities contained in the buffer gas that is independent of the pump power, and a contribution γ_1 caused by radiation trapping which is proportional to the pump power. Radiation trapping becomes more important for higher vapor densities and this explains the observed dependence of the effective damping on the temperature.

C. Coated cell

The silicone-coated surface causes much weaker relaxation than the bare glass surface. This is immediately confirmed by the magnetic resonance line, which exhibits an almost Lorentzian shape, as illustrated by Fig. 7. This time we must use the complete theoretical expression of (38) for a fit of the theory to the data and include the depolarization probability ε as an additional fit parameter. The fit delivers $\varepsilon = 1.1 \times 10^{-2}$ with a statistical error of $\pm 7 \times 10^{-4}$ as estimated from the spread of the data around the theoretical curve. As indicated by the statistical error the line shape is rather sensitive to variations of ε in this case and therefore provides a way to determine the depolarization quantitatively, in contrast to the case of strong depolarization considered in the previous paragraph.

As discussed in the theoretical section, the determination of the depolarization probability depends on deviations of the experimental line shape from a Lorentzian shape. To assess the significance of these deviations, we also fitted a purely Lorentzian line to the data, thus neglecting the modifications caused by surface-induced relaxation. Figure 8 depicts the data residuals for a Lorentzian line (Fig. 8a) as compared with the residuals found with wall relaxation included according to (38) (Fig. 8b). Clear systematic deviations are visible in the case of the Lorentzian line. They are completely removed and only noise is left if the line shape predicted by (38) is used instead.

As in the case of the uncoated cell, we again studied the dependence of the magnetic resonance signal on the power of the pump beam. For several powers between 1 and 20 mW corresponding to light intensities of roughly 5 to 100 mW/cm^2 we measured the magnetic line and extracted the depolarization probability ε, the nominal pump rate P_0, and the effective damping rate γ_{eff}, which are depicted in Fig. 9. The depolarization probability stays fairly stable over the range of powers investigated, as one would expect provided that the light does not change the properties of the silicone coating. In Fig. 9a it is only the data point at 20 mW that shows a significant deviation. However, over several data runs the value of ε turned out to vary by more than a factor of two, which clearly exceeds the fluctations expected from the statistical noise. These variations seem to be partly correlated with the pump power, in that ε shows a tendency to increase with the pump power. The underlying reason is not clear. Both the possibility that there is some minor deficiency of the theoretical description producing a systematic error as well as the possibility that the behavior of the spin-polarized atoms at the surface indeed changes have to be considered.

While the variations of the depolarization probability are relatively moderate, the nominal pump rate determined from the experimental data shows a rather

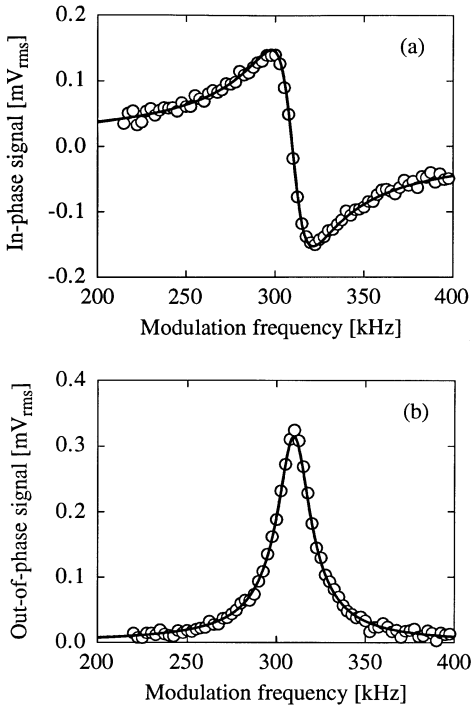

Fig. 7a, b. In-phase (**a**) and out-of-phase (**b**) magnetic resonance signal measured with the silicone-coated glass cell in the region of partial transmission at a pump power of 10 mW. Only every tenth data point is depicted. The *solid curves* represent a simultaneous least-squares fit of the theory to both signals. Constant backgrounds have been subtracted from the experimental data. The fit indicates that the depolarization probability per wall collision is approximately 0.011

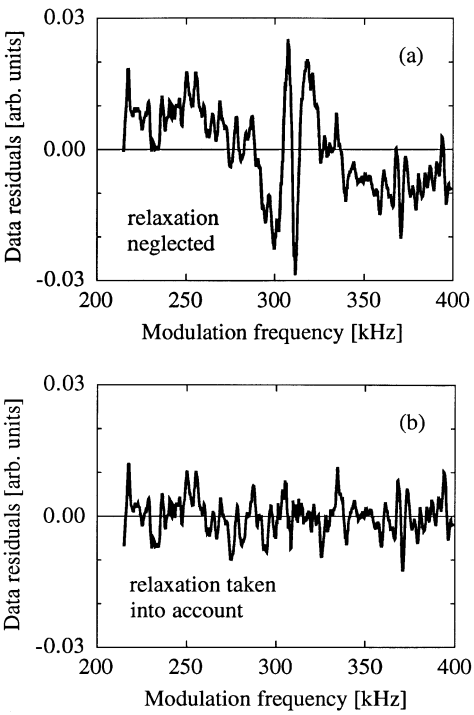

Fig. 8a, b. Data residuals obtained when a Lorentzian line is fitted to the data shown in Fig. 7a, which means that wall relaxation is neglected (**a**), as compared with the residuals delivered by a fit taking into account the modification of the line shape caused by wall relaxation (**b**)

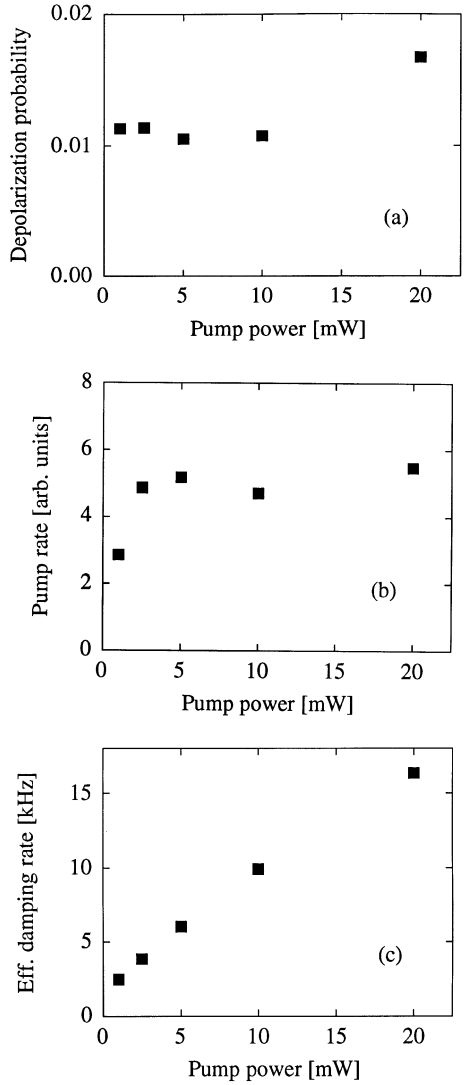

Fig. 9a–c. Depolarization probability (**a**), pump rate (**b**), and effective damping rate (**c**), as extracted from magnetic resonance lines recorded with the silicone-coated cell at different powers of the pump laser beam

dramatic deviation from the behavior expected. For the smallest pump powers used it rises with increasing power, but then it stays more or less constant, in clear contrast to the expectation that it should be proportional to the pump power. The effect is rather striking, as the absolute magnitude of the signal even decreases although the atomic vapor is optically more strongly pumped. One should keep in mind that the experimental parameter plotted in Fig. 9b also contains the density of the Na vapor, so the observed behavior could be caused by a decrease of the vapor density with increasing pump power. It is known from experiments by Gozzini et al. and M. Meucci et al. that silicone layers of the type used here can show strange effects [34, 35]. These groups reported the observation of light-induced ejection of alkali atoms from such layers in alkali vapor cells. This effect was observed even for very weak light intensities and resulted in vapor densities by far large than expected from the equilibrium

vapor pressure. There is no obvious correlation between this effect and the behavior observed in our experiment, where the vapor density seems to decrease with increasing light power, but one may nevertheless speculate that the effects might be related to one another. A clear indication that the silicone layer has some influence on the Na density in our experiment is provided by the observation that the vapor density at a given temperature was much lower in this cell than in the uncoated one. Moreover, it increased considerably more slowly with temperature than expected from the vapor pressure curve [31]. It should be pointed out, that in our cell Na was partly deposited directly onto the silicone-coated walls during the filling procedure, a situation which according to Gozzini et al. prevents photoejection.

In contrast to the pump rate (or, as pointed out above, rather the pump rate times the Na density) the effective damping rate extracted from the experimental data (Fig. 9c) shows no strange behavior, but is rather in agreement with the expectation that it should increase linearly with the pump power. The extrapolated value for zero power is close to the value observed with the uncoated cell. For higher pump powers the values are smaller than in the measurement presented in Fig. 6, but this can at least qualitatively be attributed to the fact that the measurements with the coated cell were performed at a smaller Na vapor density, so radiation trapping should contribute less to the effective damping.

VI. Conclusions and outlook

The experimental method presented in this paper provides a novel tool for studying spin relaxation at surfaces. Optical preparation and detection of the spin polarization ensure a very high sensitivity, making possible the study of the spin polarization in a thin surface layer of a dilute atomic vapor containing only $\sim 10^5$–10^6 Na atoms. Polarization-modulated optical pumping in a transverse static magnetic field allows us to perform a magnetic resonance experiment in this configuration, using a laser beam for detection that is reflected at the surface under study. In the steady state the wall relaxation leads to a spatially inhomogeneous magnetization across a layer close to the wall, in which the individual atoms show a transient behavior when their polarization is built up again after depolarization at the surface. This inhomogeneous layer reveals itself as a characteristic modification of the shape of the magnetic resonance line, which directly reflects the strength of the depolarizing atom-surface interaction.

The experimental results obtained with bare and silicone-coated glass surfaces provide a clear confirmation that the basic features of the system are properly described by the theory worked out in Sect. III. The theory not only gives the correct magnetic line shape in both cases, but also gives a correct description of the optical line shape, as discussed in [18]. The evaluation of the experimental observations both with regard to the magnetic and the optical resonance give consistent results concerning the depolarizing properties of the two surfaces studied.

For the bare glass surface quantitative information about the depolarization at the surface is provided by the optical resonance. The dependence of the optical line shape on the angle of incidence immediately below the critical angle of total internal reflection indicates that the depolarization probability ε per wall collision is approximately 0.5 [18]. Under our experimental conditions, this means that the magnetization at the wall is a fraction $g_0 = 0.03$ of the bulk value for a typical effective damping rate $\gamma_{\text{eff}} = 2\pi \times 10\,\text{kHz}$. In this case the theory predicts that the magnetic resonance line has a shape which is almost independent of the exact numeric value of ε. Indeed, the experimental line shape is very well described by this asymptotic form. Although we cannot get accurate information about the wall relaxation from the magnetic resonance line in this case, it nevertheless provides an interesting possibility for studying the relaxation in the vapor itself. As we probe only atoms close to the surface, i.e., in a thin layer at the outer boundary of the vapor, we may expect a different behavior than in the bulk, especially with regard to the radiation trapping [32, 33]. Such studies could be an interesting extension of the measurements presented above.

To extract quantitative information about ε from the magnetic resonance line in the region $\varepsilon > 0.1$ it is crucial to measure as far as possible into the wings of the line ($\delta \gg \gamma_{\text{eff}}$), where the deviations from the asymptotic line shape are most pronounced. Furthermore, it is essential to control the out-of-phase background thoroughly, so that this parameter need not be fitted, but can be inferred from an independent measurement. With these measures future experiments should allow us to extend the range quantitatively accessible via the magnetic resonance to values well above 0.1.

In the case of the weakly depolarizing silicone-coated glass surface the situation is reversed. Here, the magnetic resonance gives the more accurate information about the depolarization as compared with the optical resonance. From the latter we could only put an upper boundary on ε of roughly 0.04 [18], whereas the analysis of the magnetic resonance presented in this paper indicates that ε is approximately 0.01, which corresponds to $g_0 = 0.7$ at $\gamma_{\text{eff}} = 2\pi \times 10\,\text{kHz}$. In summary, we thus find that the two aspects of the experiment, namely the optical and the magnetic resonance, are complementary to one another with regard to the information they provide about the depolarization probability ε. For strong depolarization the optical resonance is more sensitive, whereas for weak wall relaxation the magnetic resonance represents the better tool for the determination of ε.

For the silicone-coated cell we found a strange dependence of the signal amplitude on the pump power, which possibly indicates that the Na density changes. To clarify this behavior future measurements should include the variation of several parameters such as temperature, powers of the pump and probe beam, buffer gas pressure, etc.. The question should be addressed, whether the observed effect is related with observations reported by other authors [34, 35]. Furthermore, for checking the reliability of the method described in this paper, a direct comparison with other, more conventional methods for studying wall relaxation would be helpful.

A further development of the method as a surface-physical tool with an extension to other surfaces seems promising. For example, the study of the temperature dependence of the wall interaction provides information about activation energies for desorption and surface diffusion, as has been demonstrated by other experiments [3, 4]. The method presented here offers the advantage that it only probes the illuminated area and therefore also can be applied to rather small surface samples, including single-crystal surfaces.

This research was supported by the Schweizerischer Nationalfonds and a "human capital and mobility" grant from the Bundesamt für Bildung und Wissenschaft (contract no. 93.0231). Assistance from Tilo Blasberg is gratefully acknowledged.

References

1. Slichter, C.P.: Ann. Rev. Phys. Chem. **37**, 25 (1986)
2. Kwon, T.M., Mark, J.G., Volk, C.H.: Phys. Rev. A **24**, 1894 (1981)
3. Wu, Z., Happer, W., Kitano, M., Daniels, J.: Phys. Rev. A **42**, 2774 (1990)
4. Butscher, R., Wäckerle, G., Mehring, M.: J. Chem. Phys. **100**, 6923 (1994)
5. Bouchiat, M.A., Brossel, J.: Phys. Rev. **147**, 41 (1966)
6. Happer, W.: Rev. Mod. Phys. **44**, 169 (1972)
7. Chmelka, B.F., Raftery, D., McCormick, A.V., de Menorval, L.C., Levine, R.D., Pines, A.: Phys. Rev. Lett. **66**, 580 (1991)
8. Sachleben, J.R., Wooten, E.W., Emsley, L., Pines, A., Colvin, V.L., Alivisatos, A.P.: Chem. Phys. Lett. **198**, 431 (1992)
9. Widdra, W., Detje, M., Ebinger, H.-D., Jänsch, H.J., Preyss, W., Reich, H., Veith, R., Fick, D.: Rev. Sci. Instrum. **66**, 2465 (1995)
10. Ebinger, H.D., Detje, M., Jänsch, H.J., Polenz, C., Polivka, B., Preyss, W., Saier, V., Veith, R., Fick, D.: Surf. Sci. **331-333**, 759 (1995)
11. Burgmans, A.L.J., Woerdman, J.P.: J. Phys. **37**, 677 (1976)
12. LeBoiteux, S., Simoneau, P., Bloch, D., Ducloy, M.: J. Phys. B **20**, L149 (1987)
13. Oria, M., Chevrollier, M., Bloch, D., Fichet, M., Ducloy, M.: Europhys. Lett. **14**, 527 (1991)
14. Ducloy, M.: Opt. Commun. **99**, 336 (1993)
15. Suter, D., Äbersold, J., Mlynek, J.: Opt. Commun. **84**, 269 (1991)
16. Grafström, S., Blasberg, T., Suter, D.: J. Opt. Soc. Am. B **13**, 3 (1996)
17. Grafström, S., Suter, D.: Opt. Lett. **20**, 2134 (1995)
18. Grafström, S., Suter, D.: Phys. Rev. A (in print)
19. Suter, D., Mlynek, J.: Phys. Rev. A **43**, 6124 (1991)
20. Klepel, H., Suter, D.: Opt. Commun. **90**, 46 (1992)
21. Suter, D., Mlynek, J.: Laser excitation and detection of magnetic resonance. In: Warren, W.S. (ed.). Advances in magnetic resonance, vol. 16, p. 1. New York: Academic Press 1991
22. Suter, D.: Optically enhanced magnetic resonance. In: Grant, D.M., Harris, R.D. (eds.). Encyclopedia of nuclear magnetic resonance. Chichester: Wiley 1995
23. Allegrini, M., Bicchi, P., Moi, L., Savino, P.: Opt. Commun. **32**, 396 (1980)
24. Tanaka, M., Ohshima, T., Katori, K., Fujiwara, M., Itahashi, T., Ogata, H., Kondo, M.: Phys. Rev. A **41**, 1496 (1990)
25. Alison Flood, E. (ed.): The solid-gas interface, vol. 2. New York: Marcel Dekker 1967
26. Masnou-Seeuws, F., Bouchiat, M.-A.: J. Phys. (Paris) **28**, 406 (1967)
27. Wu, Z., Schaefer, S., Cates, G.D., Happer, W.: Phys. Rev. A **37**, 1161 (1988)
28. Nienhuis, G., Schuller, F., Ducloy, M.: Phys. Rev. A **38**, 5197 (1988)
29. Born, M., Wolf, E.: Principles of optics, 5th edn. Oxford: Pergamon 1975
30. Borchers, H., et al. (eds.): Landolt-Börnstein Zahlenwerte und Funktionen aus Physik, Chemie, Astronomie, Geophysik und Technik, 6th edn., vol II, Sect. 5a, p. 536. Berlin: Springer 1969
31. Hultgren, R., et al. (eds.): Selected values of the thermodynamic properties of the elements. Metals Park: American Society for Metals 1973
32. Tupa, D., Anderson, L.W., Huber, D.L., Lawler, J.E.: Phys. Rev. A **33**, 1045 (1986)
33. Mori, Y., Takagi, A., Ikegami, K., Fukumoto, S., Ueno, A., Levy, C.D.P., Schmor, P.W.: Nucl. Instrum. Methods Phys. Res. A **268**, 270 (1988)
34. Gozzini, A., Mango, F., Xu, J.H., Alzetta, G., Maccarrone, F., Bernheim, R.A.: Il Nuovo Cimento D **15**, 709 (1993)
35. Meucci, M., Mariotti, E., Bicchi, P., Marinelli, C., Moi, L.: Europhys. Lett. **25**, 639 (1994)